Nuclear Inst. and Methods in Physics Research, A 903 (2018) 297–301

Contents lists available at ScienceDirect

Nuclear Inst. and Methods in Physics Research, A

journal homepage: www.elsevier.com/locate/nima

A 4.5 μm PIN diamond diode for detecting slow neutrons

Jason Holmes [a], Maitreya Dutta [b], Franz A. Koeck [a], Manpuneet Benipal [a], Jesse Brown [a], Benjamin Fox [a], Raghuraj Hathwar [c], Holly Johnson [a], Mohamadali Malakoutian [b], Mehdi Saremi [c], Anna Zaniewski [a], Ricardo Alarcon [a,*], Srabanti Chowdhury [b], Stephen M. Goodnick [c], Robert J. Nemanich [a]

[a] Department of Physics, Arizona State University, Tempe, AZ 85287-1504, United States
[b] Department of Electrical and Computer Engineering, University of California, Davis, CA 95616, United States
[c] School of Electrical, Computer and Energy Engineering, Arizona State University, Tempe, AZ 85287-9309, United States

ARTICLE INFO

Keywords:
Diamond detector
PIN diode
Charge collection
Neutron detection
Radiation hardness

ABSTRACT

The response of a PIN diamond diode with a 4.5 μm thick i-layer to α-particles from a ^{210}Po radioactive source has been measured and compared to the response from a 300 μm thick single crystal type IIa diamond. The results show that this PIN diamond diode with thin i-layer can be employed to detect slow neutrons following absorption on a converter boron layer. Such a detector will operate at low voltages and be rather insensitive to gamma background and neutron radiation damage.

1. Introduction

Diamond has very promising properties for a radiation detector and diamond detectors under α-particle irradiation have shown 100% charge collection efficiency and a resolution <1% [1]. For instance, the detection of slow neutrons, with energies below 0.5 eV, can be effectively accomplished by depositing a thin layer (converter) of boron onto a single crystal diamond that acts as the charged particle detector [2]. Detection of slow neutrons is of particular significance in present day commercial nuclear reactors as well as in basic research at spallation sources and research reactors. The measurement of neutron flux distribution at many points in any reactor is the first step in calculating and setting the most economical operating power, and it is considered critical input for reactor safety and reactor control systems. Out-of-core sensors are the usual basis of reactor control and safety channels, with typical ranges covered by out-of-core neutron detectors going from 10^0 to 10^{10} n cm^{-2} s^{-1} depending on the reactor power range [3]. In general, compactness and miniaturization are key requirements of any detector system that seeks to compete with neutron sensors of the gas-filled type such as BF_3 proportional counters, ^{10}B-lined detectors and ^{3}He proportional counters. These detectors offer wide dynamic range, long-term stability, and resistance to radiation damage [3].

In this paper we propose detecting slow neutrons by attaching the converter to a diode with a very thin intrinsic diamond layer, initially with an active area of about 8 mm^2. The detecting layer will be ultra-thin (about 1–2 orders of magnitude thinner than using a single crystal diamond such as those of ref. [2]) which will make it essentially insensitive to gamma radiation, a unique advantage for neutron detectors. It will provide low voltage operation (<10 V) thus enabling a compact design and real time measurements, and high stability and operation within a wide range of radiation environments due to the high damage threshold and thermal stability of diamond as a semiconductor. As a first step in realizing the proposed detector a 4.5 μm PIN diamond diode has been designed, constructed and then tested using a flux of mono-energetic 5.3 MeV α-particles from a ^{210}Po radioactive source. The basic properties of the detector are presented in Section 2 together with aspects of the PIN diode fabrication process. In Section 3 the characterization of the detector is presented in terms of its current–voltage response and its charge collection efficiency. The response to the α-particle radiation is presented in Section 4 and a summary is presented in Section 5.

2. Design and fabrication

The ^{10}B(n,α)^{7}Li reaction is the most common reaction for the conversion of thermal and slower neutrons: it is predominantly given by $^{10}_5B + n \rightarrow {}^4_2He\,(1.47\ MeV) + {}^7_3Li(0.84\ MeV)$ corresponding to a 94% branching ratio leaving the reaction product ^{7}Li in its first excited state. The thermal neutron absorption cross section is about 3500 barns and the energies of the α-particle and ^{7}Li nuclei are 1.47 MeV and

* Corresponding author.
E-mail address: ralarcon@asu.edu (R. Alarcon).

https://doi.org/10.1016/j.nima.2018.06.061
Received 8 May 2018; Received in revised form 12 June 2018; Accepted 21 June 2018
Available online 23 June 2018
0168-9002/

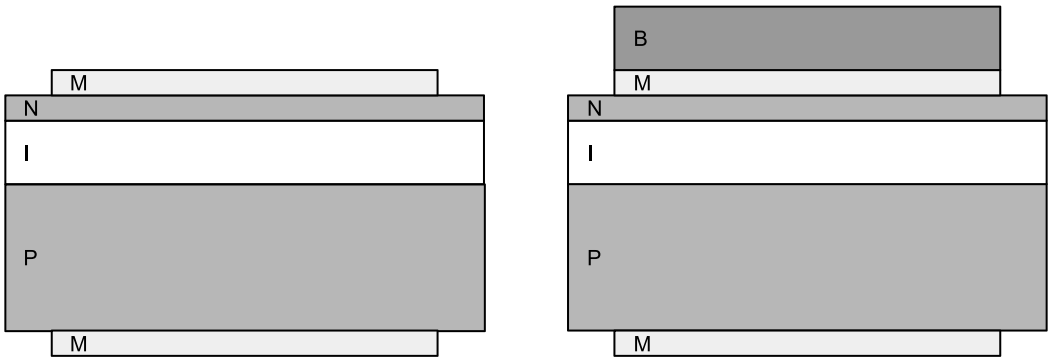

Fig. 1. Schematic of the proposed detector for slow neutrons (M: metal contact, P: p-layer, N: n-layer, I: Intrinsic layer, B: Boron converter layer). The left figure corresponds to the PIN diode presented in this paper while the right figure is the proposed slow neutron detector with a boron converter layer.

0.84 MeV, respectively. Fig. 1(right) shows a schematic of the proposed detector. Neutrons absorbed in the ^{10}B conversion layer are detected by measuring the energy deposited by one of the decay charged particles in the intrinsic diamond layer.

The optimal thickness of the ^{10}B layer is close to, but less than, the range of the 1.47 MeV α-particles in ^{10}B which is just 3.62 μm. The range in diamond of the 1.47 MeV α-particle is very close to that in ^{10}B so its detection can indeed be accomplished with a very thin PIN diamond diode. The maximum theoretical efficiency for thermal neutrons of the arrangement depicted in Fig. 1 has been calculated to be about 6% although experimental verification came up short by about an order of magnitude [4]. The detector will be designed to operate in pulse mode for initial detection rates up to 100 kHz. Operations at much higher neutron flux (about 10^{12} n cm^{-2} s^{-1}) can be achieved in pulse mode by using a very thin converter layer (about 50 nm), an active detection area of 0.5 mm by 0.5 mm and by optimizing the read-out electronics to handle detection rates up to 100 MHz. Current mode operation is limited only by the radiation hardness of the device, a property that makes diamond the best choice among semiconductor diode detectors. The construction and performance of the PIN diode shown in Fig. 1 (left) is described in this paper. This PIN diode lacks the conversion layer but its performance can be evaluated by using α-particles with kinetic energies similar to the ones coming from the $^{10}B(n,\alpha)$ ^{7}Li reaction.

The PIN detector diode was prepared using 3 mm × 3 mm × 0.3 mm high-pressure, high-temperature (HPHT), boron doped substrates with a boron concentration of ~1.2×10^{20} cm^{-3}. With a crystallographic (111) orientation and minimum miscut angle of ±1.5 deg, the surface was polished to an Ra of ~40 nm. Prior to diamond layer deposition the substrate was cleaned using a three step wet-chemical process with a boil in $H_2SO_4/H_2O_2/H_2O$, 3:1:1 at 220 °C for 15 min, HF treatment for 5 min, and a final boil in $NH_4OH/H_2O_2/H_2O$, 1:1:5 at 75 °C for 15 min. After each step the substrate was rinsed with DI water, and finally dried with N_2 before transfer into the CVD reactor for growth of intrinsic diamond. This intrinsic diamond CVD system is dedicated to growth of undoped diamond. The chamber base pressure in the low 10^{-8} Torr regime is achieved with oil free pumping, and the diamond deposition process employs an oil free positive displacement pump. The intrinsic diamond layer growth used research grade hydrogen, methane and 6N oxygen. A dual-wavelength (2.1/2.4 μm) optical pyrometer was employed for temperature control and film thickness measurement. Heating of the substrate was achieved through exposure to the plasma discharge taking advantage of plasma focusing and a water cooled sample stage.

Prior to intrinsic diamond growth the diamond substrate was exposed to a pure hydrogen plasma at a temperature of ~800 °C for 5 min. The intrinsic diamond layer was grown using 392 sccm hydrogen, 7 sccm methane and 0.75 sccm oxygen at a chamber pressure of 65 Torr and a microwave power of 1200 W establishing a growth temperature of 800–850 °C. Under these growth conditions the main impurity is nitrogen with a concentration of ~7×10^{15} cm^{-3}. For the successive, n-type, phosphorus doped diamond layer, the sample was loaded into a dedicated phosphorus doping CVD system operating with oil free pumping similar to the intrinsic system and using a 200 ppm trimethylphosphine (TMP) in hydrogen gas mixture as the dopant source. After an initial surface cleaning step by exposure to a pure hydrogen plasma the phosphorus doped layer was grown establishing flow rates for hydrogen, TMP-hydrogen and methane of 350 sccm, 50 sccm and 0.5 sccm, respectively. At a chamber pressure of 60 Torr and microwave power of 2000 W, a temperature of about 900 °C was measured. From similarly grown films a thickness of about 400 nm and a phosphorus concentration of ~5×10^{19} cm^{-3} was derived from SIMS results.

The first step in the fabrication of the device shown in Fig. 1 (left) involved Oxygen (O)-terminating the surface. This is done to avoid surface conduction resulting from the formation of a two-dimensional hole gas once the sample is exposed to air post hydrogen plasma in the diamond growth reactor [5]. The procedure used has been described in ref. [6]. Prior to contact deposition, an O-plasma ash step was performed using a Tegal Oxygen asher at 200 W power and 400 mTorr pressure to ensure a pristine surface for the metal deposition. The contacts were deposited using a Lesker PVD75 e-beam metal deposition system. A shadow mask was used to prevent metal deposition along the side walls of the sample. The metal stack consisted of Ti/Pt/Au :: 50 nm/50 nm/150 nm. Ti was used for better adhesion, Au to prevent oxidation of Ti and Pt as a barrier to prevent formation of a high resistance Ti–Au intermetallic [6]. The diamond plate detector used the same contact metallization on a commercially obtained, electronic grade, (100) single crystal diamond type IIa 3 mm × 3 mm plate.

3. Device characterization

The 4.5 μm PIN diode was characterized first by measuring the PIN current–voltage (I–V) curve. This was followed by a measurement of the charge collection efficiency using the 5.3 MeV α-particle radiation coming from the ^{210}Po radioactive source.

3.1. The IV response

The IV curve was found by placing a potential difference on the PIN diamond and measuring the current. The diamond diode was biased using an ORTEC 428 detector bias supply. The current was measured with an adjustable transimpedance amplifier (TIA) made with Linear Technologies operational amplifiers [7]. The TIA voltage output is converted to a current using the known transimpedance of the amplifier, which is configurable with sensitivities ranging between 1 V/μA and 1 V/nA. The resulting I–V response is shown in Fig. 2. The curve indicates that the diamond is indeed behaving as a diode and that the turn-on voltage is at ~4.0 V.

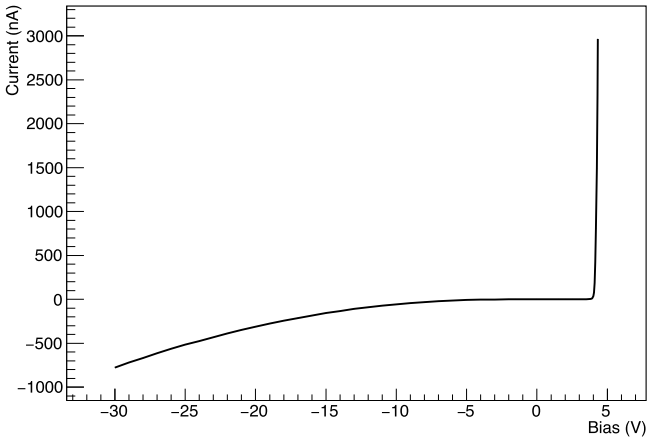

Fig. 2. I–V response of the PIN structure showing diode characteristics with a turn-on voltage of 4.5–5 V.

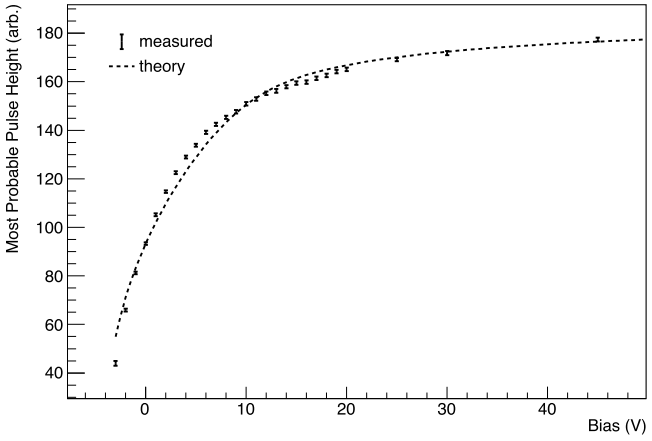

Fig. 3. The pulse height values from α-particle radiation from 210 Po as a function of the voltage applied to the 4.5 μm PIN diamond diode. The measured points are compared with simulation.

For the measurement of the thickness of the intrinsic layer, the capacitance was measured as a function of the DC bias on the p-type layer using a 30 mV rms AC signal at 30 kHz. The DC bias on the substrate was swept from +6 V to −30 V. The measurement was performed with a Keithley 4200 SCS Parameter Analyzer. Assuming a relative permittivity of 5.7 and an active area of 3 mm × 3 mm, the thickness of the intrinsic-layer was calculated to be at least 4.46 μm using the value of normalized capacitance at −30 V. The V_{bi} was found to be ~4.5–5 V which is similar to the observed turn on voltage in the IV response and consistent with our earlier reports of bipolar transport in our devices [6].

3.2. Charge collection

To measure the charge collection efficiency the 4.5 μm PIN diamond diode was connected to a standard pulse counting electronics system. The signal connection was fed into an ORTEC 142A preamplifier and the output connected to an ORTEC 672 spectroscopy amplifier. The n-side of the diamond diode was biased between −3 V and 45 V relative to the p-side (reverse bias is positive) using the ORTEC 428 detector bias supply. The p-side was biased to ground and the response to the α-radiation from the ^{210}Po source was also measured from the n-side.

Pulse height distributions were collected for the above biases and the most probable value for each distribution, corresponding to the most probable energy deposit or energy peak, was selected and plotted versus the bias. The results are shown in Fig. 3. The experimentally observed charge collection efficiency curve can be accurately reproduced by modeling the pin diamond detector using Silvaco ATLAS, a commercial semiconductor device simulator modified here for diamond materials. The alpha particle induced electron–hole generation rate as a function of width in diamond was obtained using the TRIM (Transport of Ions in Matter) Monte Carlo simulator for high energy particles in solids. The initial rise at low voltage is well described by the Hecht equation [8] assuming a mobility-lifetime ($\mu\tau$) product for holes of 8×10^{-8} cm^2/V in the intrinsic layer. The lack of a strong saturation at large voltages deviates from the Hecht model, and can be reproduced in ATLAS by including 10^{14} cm^{-3} donor impurities in the intrinsic layer. The presence of the donors in the intrinsic layer results in only partial depletion of intrinsic region, which reduces the effective width of the I-region, which becomes fully depleted with increasing applied voltage as compared to an ideal intrinsic layer.

4. Results

The responses to the mono-energetic α-particle from ^{210}Po were measured for the 4.5 μm PIN diode and also for a commercial, undoped, 300 μm single crystal diamond, both with the above described pulse mode electronics. The main components of the experimental setup are illustrated in Fig. 4. The detectors and the ^{210}Po source were mounted inside a vacuum chamber (808 ORTEC). A collimator (6 mm long with a 300 μm diameter aperture) was placed in front of the source. The operating vacuum was around 30 mTorr.

The ^{210}Po source is a rectangular foil with an active area of 17.8 mm x 5.1 mm, an activity of 250 μCi, and is sealed by 1.778 μm of gold metal. Because the ^{210}Po is sealed within a gold layer, the 5.3 MeV α-particles lose some energy and gain a spread in energy due to the straggling effect. We have used the code SRIM (Stopping and Range of Ions in Matter) [9] to model the effect of the gold foil on the alpha particles. Fig. 5 combines SRIM results obtained for both the doped 4.5 μm PIN diode and the undoped 300 μm single diamond, the latter used to capture the full energy coming from the source detected with higher resolution. Thus the mean energy of alphas emitted normal to the seal plane was found to be 4.490 MeV with a standard deviation σ of 30 keV or 0.7%. The 0.7% σ amounts to the straggling obtained using the Bohr's formula [10,11] which is known to be lower than the σ from the experimental data on MeV-range α-particle straggling though metal foils [12,13].

The mean energy deposit in the 4.5 μm detector is about 1.6 MeV and it is shown in Fig. 5 by the left (red) histogram. Thus, the 1.47 MeV α's emitted following neutron capture from a Boron converter will stop in the 4.5 μm diamond detector.

The experimental results are shown in Fig. 6 which combines the measured results of the pulse height distributions obtained for both the doped 4.5 μm PIN diode and the undoped 300 μm single crystal diamond plate. The α's deposit all of their energy in the 300 μm single diamond and this is shown by the black histogram of Fig. 6. From Fig. 6, taking the ratio of the peak values of the distributions one obtains 2.77 ± 0.26. This is in agreement with the SRIM calculated value from Fig. 5 for the ratio of the full energy to the energy deposit in the PIN diode, namely 2.75 ± 0.10, with the latter uncertainty being a lower limit.

The mean energy deposited in the PIN was approximately 1.6 MeV and its detection was achieved with almost no background and an 8% standard deviation dominated by the straggling in the source gold foil and in the 4.5 μm PIN diamond. On this PIN diode one can deposit a layer of boron and effectively create a slow neutron detector by detecting α-particles with energies ≤1.47 MeV.

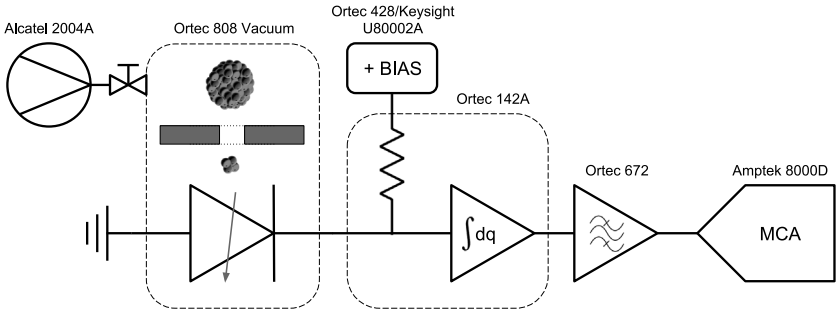

Fig. 4. A schematic of the testing apparatus indicating the vacuum chamber and associated electronics.

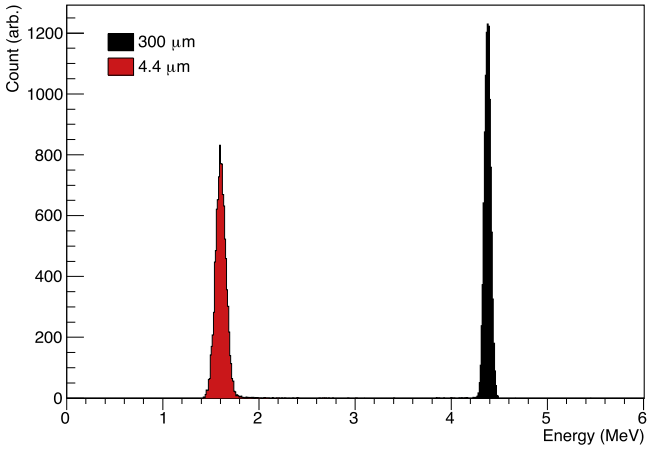

Fig. 5. Pulse height distributions for the response to 4.490 ± 0.033 MeV α-particles emitted from a sealed 210 Po radioactive source as simulated by the code SRIM. The left histogram is for a 4.5 μm PIN-doped diamond diode. The right histogram is for an undoped 300 μm single crystal diamond.

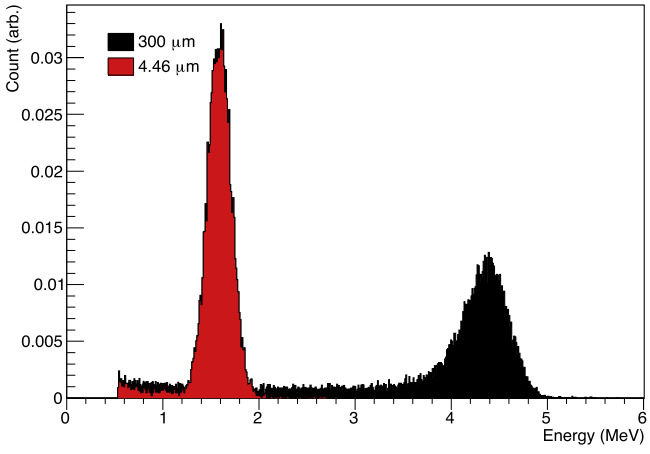

Fig. 6. Pulse height distributions for the response to 4.5 ± 0.1 MeV α-particles emitted from a sealed 210 Po radioactive source. The left histogram is for a 4.5 μm PIN-doped diamond diode. The right histogram is for an undoped 300 μm single crystal diamond.

5. Summary

A 4.5 μm PIN diamond diode has been constructed and tested with a beam of α-particles coming from a sealed ^{210}Po source. The junction behaves like a diode detector with a turn-on voltage of 4.0 V. If the detector is forward biased at or beyond the turn-on voltage, the diode no longer operates as a detector. The doping of the diode introduces an intrinsic electric field even when no bias is applied. Due to the diamond being so thin, 4.5 μm, the intrinsic field strength is nearly 1 V/μm, which may be sufficient for pulse-counting mode and would not require an external bias in certain applications allowing for compact, low-power designs.

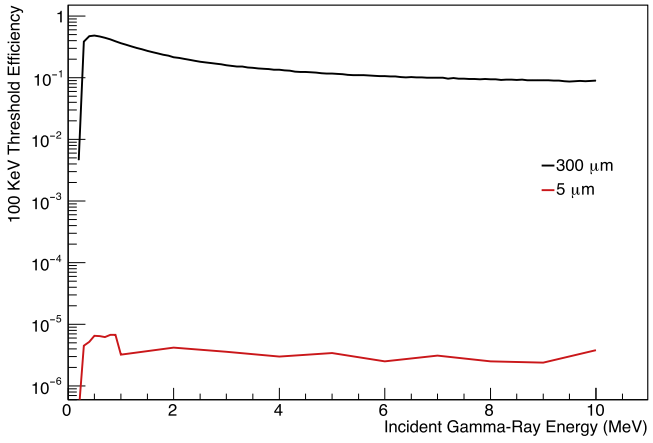

Fig. 7. Percent efficiency for gamma detection as a function of gamma energy for a 100 KeV threshold as calculated by the code GEANT4. The top curve is for a 300 μm thick diamond and the lower curve for a 5 μm thick diamond.

The next step towards a slow neutron detector includes the construction of a prototype 4.5 μm detector with a layer of about 2.5 μm of boron deposited on the surface. This detector will have initial pulse counting capabilities up to 100 kHz, an estimated 5% efficiency for thermal neutrons, and it would be rather insensitive to gamma radiation. The latter is shown in Fig. 7 by a GEANT4 calculation of the gamma efficiency for both a 5 μm and a 300 μm thick diamond, with a 100 keV threshold. Based on the neutron kerma coefficients [14] it is expected that the fluence for thermal neutrons can be about five orders of magnitude higher than that for the standard 1 MeV neutrons. Radiation damage in diamond sensors have been observed for fluences of about $10^{15} n_{1\ MeV}/cm^2$ [15]. Testing of the device is envisioned to be done shortly with a beam of thermal neutrons at the HFIR facility at Oak Ridge National Laboratory.

Acknowledgment

This work was supported by ARPA-E DE-AR0000453 through the SWITCHES program.

References

[1] J.H. Kaneko, et al., Nucl. Instrum. Methods A 505 (2003) 187.
[2] M. Angelone, et al., IEE Trans. Nucl. Sci. 56 (2009) 2275.
[3] G.F. Knoll, Radiation Detection and Measurement, John Wiley, Hoboken, N.J, 2010.
[4] M. Wielunski, et al., Nucl. Instrum. Methods Phys. Res. A 517 (2004) 240–253.

[5] S. Yamasaki, E. Gheeraert, Y. Koide, MRS Bull. 39 (6) (2014) 499–503.
[6] M. Dutta, F. Koeck, W. Li, R.J. Nemanich, S. Chowdhury, IEEE Electron Device Lett. 38 (5) (2017) 600–603.
[7] © 2017 Linear Technology, www.linear.com.
[8] K. Hecht, Z. Phys. 77 (1932) 235.
[9] J.F. Ziegler, J.P. Biersack, U. Littmark, The Stopping and Range of Ions in Solids, Pergamon Press, New York, 1985 The corresponding program package SRIM can be found at http://www.srim.org/.
[10] N. Bohr, Mat. Fys. Medd. Dan. Vid. Selsk 18 (8) (1948).
[11] H. Enge, Introduction to Nuclear Physics, in: Addison-Wesley Series in Physics, 1966, p. 188.
[12] J., R. Comfort, J.F. Decker, E.T. Lynk, M.O. Scully, A.R. Quinton, Phys. Rev. 150 (1966) 249.
[13] S. Kumar, P.K. Diwan, J. Radiat. Res. Appl. Sci. 8 (2015) 538.
[14] R.S. Caswell, J.J. Coyne, M.L. Randolph, Int. J. Appl. Radiat. Isot. 33 (1982) 1227.
[15] F. Kassel, M. Guthoff, A. Dabrowski, W. de Boer, Phys. Status Solidi A 214 (2017) 1700162.